Challenge Journal of Structural Mechanics

Research Article

Study on slope stability of frame prestressed anchor sheet pile wall with finite element strength reduction method

Amna Saeed Al-Banaa [a,*], Zhou Yong [a]

[a] *Department of Civil Engineering, Lanzhou University of Technology, Lanzhou 730050, China*

ABSTRACT

Slope stability analysis is performed in practical geotechnical engineering using the finite element method, which is an advanced method and is widely used by engineers. With the development of computer technology, it has become easy to study the slope's stability supported by frame prestressed anchor and sheet pile wall through the displacement-based finite element numerical analysis method, to calculate the safety factors. However, the expansion angle ψ' is not widely covered. In this study, PLAXIS two-dimensional finite element method is using to establish the slope model supported by frame prestressed anchor and sheet pile wall, and the influence of expansion angle on slope deformation is studied. The results show that the expansion angle has a different effect on the convergence of the two-dimensional slope model. In the model slope, a prestressed frame anchor and sheet pile wall reinforce the slope. The failure mechanisms were unclear when $\phi' = \psi'$ (flow base). Besides, when the slope has high soil strength parameters (c' or φ'), the expansion angle will affect the calculation results and convergence. In general, the expansion angle significantly influences the slope's stability and is not affected. Therefore, it was necessary to note the effect of the angle of expansion on stability.

ARTICLE INFO

Article history:
Received 26 September 2020
Revised 31 October 2020
Accepted 10 December 2020

Keywords:
Sheet pile wall
Prestressed anchors
Safety factor
Dilatancy angle
Finite element method

1. Introduction

Slope stability analysis is a hot issue that scientists have debated since the advent of geotechnical engineering (Griffiths and Marquez, 2007). Research on slope stability and prevention of landslides has become a very important topic in geotechnical engineering. In addition, due to the regional limitations of slopes, complexity of geotechnical materials and diversity of surrounding environmental conditions; transition from the stable to the unstable, and from the hazardous state to the landslide become very complex. Therefore, how to accurately analyze and study rocks and soils requires detailed research. Soil slope stability and precise determination of landslide are the subjects of historical research (Davis, 1968; Griffiths, 1999).

When studying slope stability, several methods can be used to assess the ramp safety factor. The marginal equilibrium analysis (LE) provides values for FS on the predetermined failure surface of the circular roof (Bishop, 1955; Morgenstern and Price, 1965). The slope considers itself as a solid body with the force determined by the Mohr-Coulomb parameters and *c*. Due to the determination of its strength to the nature, the fault surface corresponding to the lowest constant service level is repeatedly determined. However, this does not guarantee that the solution represents a sliding surface with the slightest safety factor. The upper and lower limits of energy balance and static equilibrium are estimated by boundary analysis (LA). With the help of the finite element method (FEM), even for complex problems (Lyamin and Sloan, 2002a; 2002b); these limits can be determined (Sulsky et al., 1995) as well as inserted instability analysis (Zabala and Alonso, 2011). Slope stability is measured by analysis of slope stability using the finite element method. There are several methods for the assessment of a safety factor. The surface fault corresponding to the minimum fixed service is determined in an iterative manner. In the finite element method, stability of the slope is determined by force.

* *Corresponding author*. Tel.: +86-189-190-33010 ; E-mail address: eng_amna20000@yahoo.com (A. S. Al-Banaa)
ISSN: 2149-8024 / DOI: https://doi.org/10.20528/cjsmec.2021.01.006

Nomenclature

Ψ	The volumetric expansion angle
ψ'	Dilatancy angle
φ	Angle of friction
φ'	Effective friction angle
c	Soil cohesion coefficient
γ	Unit weight
ν	Poisson's ratio
E	Young's modulus
FoS	Factor of safety

The reduction method (SR) was developed by (Zienkiewicz et al., 1975). They combined it with the Mohr-Coulomb model. After, Tschuchnigg et al. (2015) carried out extensive research on this problem, including the refinement of finite element mesh and the elastic-plastic flow rule. Further modifications of SR can also be found in Tschuchnigg et al. (2015). It is essential to combine staged structural modeling and stability analysis without using other tools while preserving variable stress and history. Even if the Mohr-Coulomb model can predict the stress state.

When failure occurs, the results of predicting the stress response are not ideal. The foundational modeling theories of advanced elastomeric plastics, such as compact surface plasticity and other modeling frameworks of Dafalias (1986), including Under Plastic Woo and Columba's (Wu and Kolymbas, 1990) and the Odyssey Columba's Bar (Kolymbas, 2012), were directed in order to overcome these difficulties.

Suggested, these models were further refined to capture the stiffness of niemonis, anisotropy or viscosity by Jerman and Mašín (2020). These models can consider not only the nonlinear strain response of soil but also the state and load history dependence of soil. However, methods of reducing the strength of these models are not often feasible. Therefore, if an advanced foundation model is to be used in the staging construction and stability analysis is required, the parameters must be recalibrated. The M-C model must be used.

However, if it is assumed that ψ'=0°, the following two main factors should be taken into consideration. First, the worst case is considered in the numerical analysis to obtain a low *FoS* (Manzari and Nour, 2000; Hang and Ping, 2012; Kumar, 2004). In addition, in the second case, when the soil is sheared, ultimately small (constant volume) the plastic volume of soil changes. In contrast, soil strength is overestimated when relevant flow rules are applied. This leads to overestimation and insecurity of *FoS* (Michalowski, 2002; Manzari and Nour, 2000). However, the role of ψ' is rarely discussed. Until recently, only a few researchers considered the swelling soil effect (Li et al., 2010; Griffiths and Marquez, 2007; Zienkiewicz et al., 1975). Therefore, this study takes 2D frame prestressed anchor sheet pile wall as the research object and uses the PLAXIS two-dimensional finite element method to study the influence of expansion angle.

2. Calculation of Strength Reduction Factor by the Mohr-Coulomb Model

The M-C model's stress state is limited in the principal stress space by the yield surface *F* of the hexagonal cone. Since M-C is an elastic-plastic complete plastic model, once the loading path reaches the stress state on the yield surface, the model will show a plastic strain response. At the integration point, the strength parameters decrease from the initial values of φ_1 (internal friction angle) and c_1 (cohesion) to their corresponding φ_2 and c_2, which directly reduces the size of yield surface *F*. These results in lower deviation *Q* and average stress *P* at the limit state, as shown in Fig. 1(a).

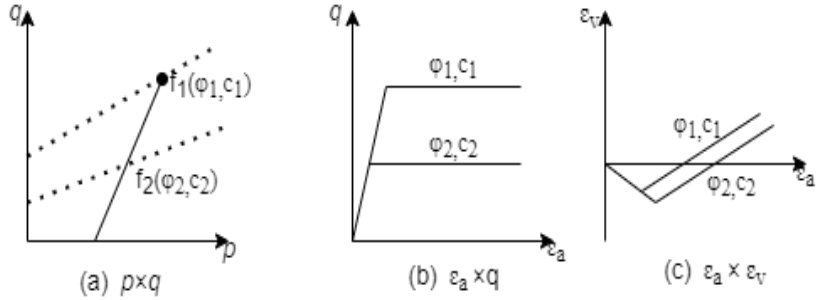

Fig. 1. Impact of force reduction on the M-C of the 3-axis dried stress.

The limit state is represented by a continuous excessive axial deformation ε_a, as shown in the Fig. 1(b). The volume strain ε_v in the limit as shown in the Fig. 1(c), state depends on the so-called flow rule controlled by the dilatancy parameter ψ. When the test stress state appears outside the yield surface, the stress recovery relies on the plastic deformation's consistent condition. In the finite element method, the strength parameters of each reduction step are evaluated as:

$$\tan \varphi_r = \frac{\tan \varphi_0}{FR} \tag{1}$$

$$c_r = \frac{c_0}{FR} \tag{2}$$

FR is the reducing factor, and the 0 and *r* which represent the initial and reduced value of a parameter, respectively. The reduction of the force coefficients finally reaches the limit state. In the finite element simulation, once the analyzer is unable to find a solution to the unbalanced force resulting from a further decrease in the material's strength, it is seen as reaching the bound state. It should not be considered that the iterative process of finding equilibrium is associated with excessive

deformation of the shear region. In any case, this deformation has no physical significance related to the reduction of the artificial force. However, the resulting displacement indicates the location of the potential shear regions. Then *FS* is calculated as:

$$FS = \frac{\tan \varphi_0}{\tan \varphi_f} = \frac{c_0}{c_f} \quad (3)$$

This means that the *FS* equation is equal to the *FR* (Eqs. (1 and 2)). The symbol *f* in Eq. (3) represents the parameter value at the time of failure. It should be not that M-C parameters can be chaos as φ>0 and *c*>0 to represent the peak state, or φ 0 and *c*=0 to predict the critical state, depending on the soil condition in the slope analyzed. Also, the behavior of the M-C model is determined by two additional parameters: Young elastic Stiffness *E* and Poisson's ratio *v*.

3. Numerical Modeling Procedure

3.1. Main parts of the prestressed anchor bar and sheet pile wall

The prestressed anchor sheet pile wall structure is mainly composed of a reinforced concrete, prestressed anchor rod, and sheet pile wall. The free part of the prestressed anchor cable is embedded in the filler and passed through the potential sliding surface, as shown in Fig. 2 the anchorage section is located in the soil, the anchor supporting structure, and the anchor head plate wall. The ground pressure load acts on the supporting system of the prestressed anchor cable wall. The external force through the anchorage section is transferred to the free area of the pile. The anchor's strength can maintain the stability of the pile sheet wall structure.

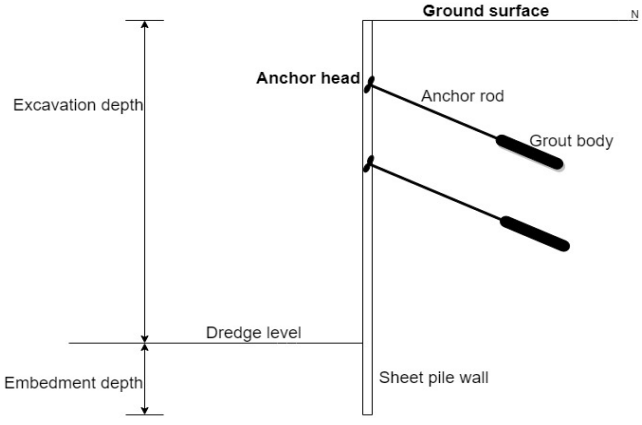

Fig. 2. Structure of the prestressed anchor bar and sheet pile wall.

3.2. Non-associated plasticity

Davis (1968) noted that only when a material has a corresponding flow law is the plastic field's stress and velocity properties. If it is $\varphi' \neq \psi$, he suggested using the force reduction parameters, c^* and φ^*, and flow rules applied in the model:

$$c^* = \beta \cdot c' \quad (4)$$

$$\tan \varphi^* = \beta \cdot \tan \varphi' \quad (5)$$

$$\beta = \frac{\cos \psi' \cos \varphi'}{1 - \sin \psi' \sin \varphi'} \quad (6)$$

Therefore, c^* and φ^* are used as input parameters in all analyzes called Davis methods.

The background of Here is a detailed strength reduction parameter. Fig. 3(a) shows an ABCD element tilted perpendicularly at an angle. The basic principle of stress and tension is also explained. It was assuming that it is coaxial and that the axes are congruent. Fig. 3(b) shows the Mohr stress circuit for a given case, where the daily pressure σ_s', the shear pressure is the stress ratio, and the failure criterion determined according to the Coulomb model.

$$\tau_s = c + \sigma_s' \tan \varphi' \quad (7)$$

The point PP on the stress circle represents the pole of the plane. Therefore, when drawing lines from PP to points (I) and (II), the stress σ'_s is found and τ_s the direction of the plane in which *s* acts. According to Davis (1968), the lines representing these directions are called the characteristic pressure lines, which is uniformly distributes in the order of the central pressure at an angle of 45°-$\varphi'/2$.

Fig. 3(c) shows the case of Mohr strain circle, where δ_{ε_1} and δ_{ε_3}. It represents the primary and secondary principal strain increments, and the increment of shear strain $\delta_{\gamma}/2$.

The expansion angle ψ can be defined if the level stress condition is assumed as follows:

$$\sin \psi' = \frac{\delta \varepsilon_{vo1}}{\delta \gamma_{max}} = \frac{\delta \varepsilon_n}{\delta \gamma_{max}} = \frac{\delta \varepsilon_1 + \delta \varepsilon_2}{\delta \gamma_{max}} \quad (8)$$

where $\delta_{\varepsilon_{vo1}}$ is the volumetric stress, and $\delta_{\gamma_{max}}$ corresponds to the maximum shear stress. The points (I) and (II) represent the points of zero direct pressure increase (δ_{ε_n}=0) and the direction in which he called δ_{ε_n}=0 empty extension lines (Kumar, 2004). When drawing lines from *Pp* to points (I) and (II), the direction of the planes perpendicular to zero is found. Thus, when drawing the horizontal lines from (I) and (II) and connecting the intersection point to the Mohr strain circuit with *Pp*, the direction of the zero extension lines is found (Davis, 1968). Assumed that the extension lines of the zero represent slip lines, or in other words, velocity characteristics (Roscoe, 1970). This assumption was firstly proposed based on experiments. These velocity properties are eliminated evenly around the principal stress direction (strain), but at 45°-$\varphi'/2$. As a result, the stress properties are sliding lines only if Fig. 4(a) of the element ABCD. Fig. 3(a) represents each characteristic of stress and speed. If stability analyzes are performed based on assumed velocity characteristics (slip lines), then the ratio of actual stress should be applied to the zero extension lines rather than the proportion of stress to harmonic stress properties. The Mohr stress circuit (Fig. 4(b)) shows that shear stress τ_k and normal stress

$\sigma_{k'}$ do not reach the Mohr-Coulomb criterion. Based on these considerations. Davis (1968) proposed the use of c^* and φ^* as an effective grip angle and effective angle of friction, respectively, at sliding planes in combination with a bound flow base. The difference between φ', φ^*, c' and c^*, respectively, is illustrated in Fig. 4(b).

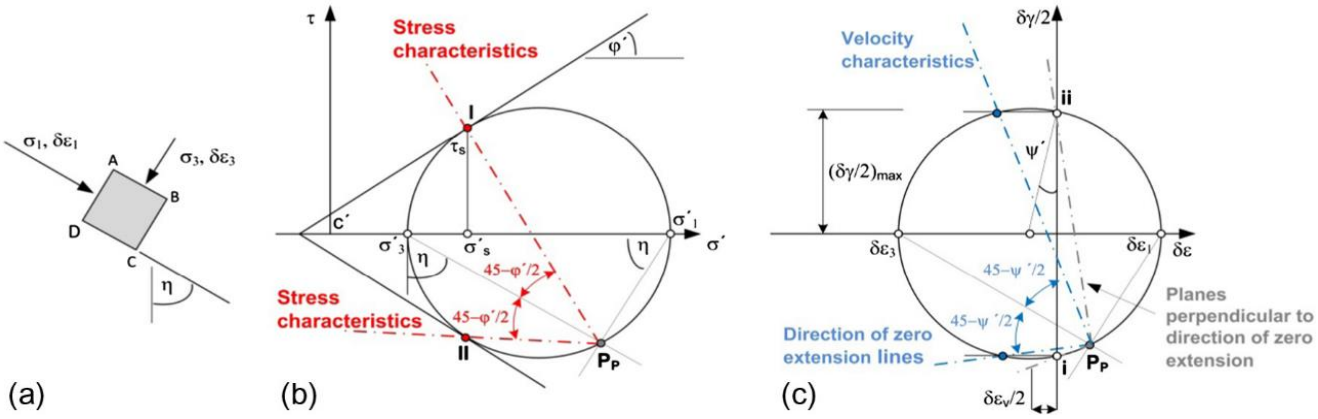

Fig. 3. (a) Considered element; (b) Stress circuit Mohr; (c) Dynasty circle Mohr.

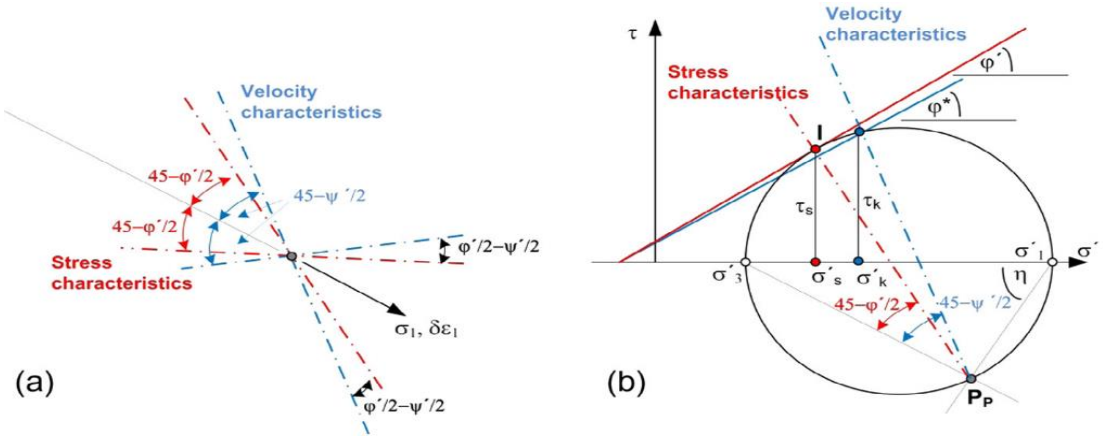

Fig. 4. Stress properties (a) with velocity (b).

3.3. Anchor bar and sheet pile wall and soil profiles

Using PLAXIS 2D software in numerical simulations. FoS safety factor was found .The analyzed results were analyzed by comparing the literature results for compatibility in three aspects: network roughness, expansion angle, and failure mechanism. In addition, after confirming that the results are reasonable and acceptable, the same as (Griffiths and Marquez, 2007). Use SRM to discuss the effects of boundary conditions, such as the geometry of the dam and the topography of the valley site, in 3D models. (Zienkiewicz et al., 1975). Parameters of throughput, including numerical calculation non-convergence, entry of plastic region, and displacement salinity at a given characteristic point, we are used to examining the *FoS* contrast ABAQUS and FLAC3D. Measures were used for the FEM model and expanded to include a pre-framed stabilizer bar and a laminate stack wall using PLAXIS 2D. Since the *FoS* was considered reasonable, The influence of the expansion angle on convergence direction discussed using different parameters (grid roughness, boundary conditions, slope angle, and soil parameters). Table 1 presents the main model parameters of an anchor framed with a sheet pile wall and Table 2 presents the soil parameters in 2D slope model.

Table 1. Main model parameters of an anchor framed with a sheet pile wall.

Items	Model	*EA* (kN/m)	*EI* (kN/m²)
Anchor	Elastic	5*106	-
Sheet pile wall	Elastic	7.5*106	1.0*106
Plate	Elastic	7.5*106	1.0*106

Table 2. Soil parameters in 2D slope model.

Parameter	Value
φ'	45°
c'	6 kPa
Ψ'	0°, 5°, 10°, 15°, 35°, 45°
E'	$1*10^5$
γ	20.20
υ	0.3

3.4. Calculations

According to the relevant flow rules, the *FoS* obtained from LAM and SRM are very close (Baker et al.,

2006). Likitlersang et al. (2018) used SRM to discuss the stability and deformation characteristics of high-speed railway embankments built on soft clay in Bangkok. The results show that most of the existing railway embankments show a greater degree of movement under a load of high-speed trains. (Cai et al., 2002) used SRM to compare the boundary effects between two-dimensional and three-dimensional models and showed that the assumed boundary conditions in the z-plane (thickness direction) are critical for three-dimensional finite element analysis, and if roller-roller Column conditions, the effect of z-direction length can be ignored. The results of ABAQUS were slightly higher than that of FLAC3D (2-4%) in the same yield. In addition, they point out that different software has different fusion standards, resulting in different FoS. Fig. 5 shows an example of a framed prestressed anchor bar and sheet pile wall.

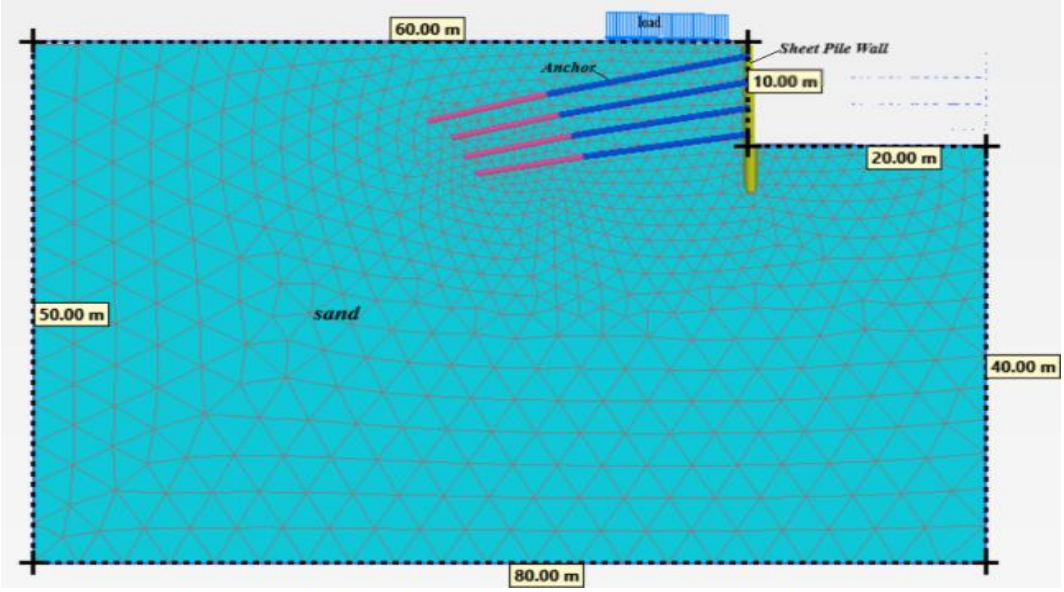

Fig. 5. An example of a framed prestressed anchor bar and sheet pile wall.

The SRM method has been used extensively in finite element geotechnical projects.

FoS solutions are integrated with SRM solutions and are a professional geotechnical specification. It was used in this study. Currently, the location of the failure surface is monitored using three standard methods, namely, joint displacement (Dafalias, 1986), plastic area (Griffiths and Marquez, 2007; Lim et al., 2015; Tschuchnigg et al., 2015) and shear stress region. As shown by Roscoe (1970) (Wu and Kolymbas, 1990), it is observed that the surface of the pores corresponds to the part of failure shear stress observed from the laboratory results.

In this study, the shear stress region is used to this monitor the position of the failure, and to compare the failure mechanisms for each of the expansion angles (ψ' = 0˚, 5˚, 10˚, 15˚, 35˚, 45˚).

4. Analysis and Results

The safety factor was checked using soil parameters and finite element method were applied to find results, a framed prestressed anchor bar and sheet pile wall for the reinforcement have been added. Fig. 1 shows an example of a framed prestressed anchor bar and sheet pile wall, and the main model parameters of an anchor framed by a wall of sheet pile are shown in Table 1, soil parameters are clarified in Table 2.

In this study, the plasticity theory was fully applied from the Mohr-Coulomb. In addition, a framed prestressed anchor bar and sheet pile wall are made in its plastic state, so that the material can be obtained and the study is done on the basis for an automatic stabilization of the slope, this modeling was done using PLAXIS 2D software.

4.1. Verification

The two-dimensional model used in this paper is the same as that used by (Tschuchnig et al., 2015). However, reinforcement with anchor was added, including slope geometry, soil characteristics element type and failure criteria (15 trigonometric node elements), as shown in Fig. 5. The network roughness, a difference in expansion angle, and failure mechanism were discussed in this paper.

SRM calculated *FoS* based on Tschuchnig et al. (2015) using five expansion angles (0°, 5°, 10°, 15°, 35° and 45°).

Moreover, ψ'=35' the compared with the prestressed frame anchor and sheet pile wall. The results in Fig. 2 show that the chances gained are 3.145 when ψ'=0°. The results (*FoS*=1.30-1.37) showed a greater trend than (Tschuchnig et al., 2015). When ψ'=45, the *FoS* affinity was irregular and low. This abnormal phenomenon is the result of destroying the uniqueness of the mechanism. The *FoS* obtained by ψ'=45˚ score 2.565 is far from

the result of Tschuchnig et al. (2015) (*FoS*=1.53). Fig. 6 shows the reason why *FoS* is greater than 45° at 35°. Possible causes of the numerical tolerances determine the content of the problem. In this research, the slope was reinforced with a framed prestressed anchor bar and sheet pile wall to reduce slips. To assess this problem, the expansion angle was studied to assess the *FoS*. If the *FoS* for ψ'=45° score between 2.565 it decreased as tolerance decreased. When tolerance decreased gradually, *FoS* increased for ψ'=35° degrees from 2.971 incidence of *FoS* at ψ'=45° was slightly lower than that at ψ'=35°.

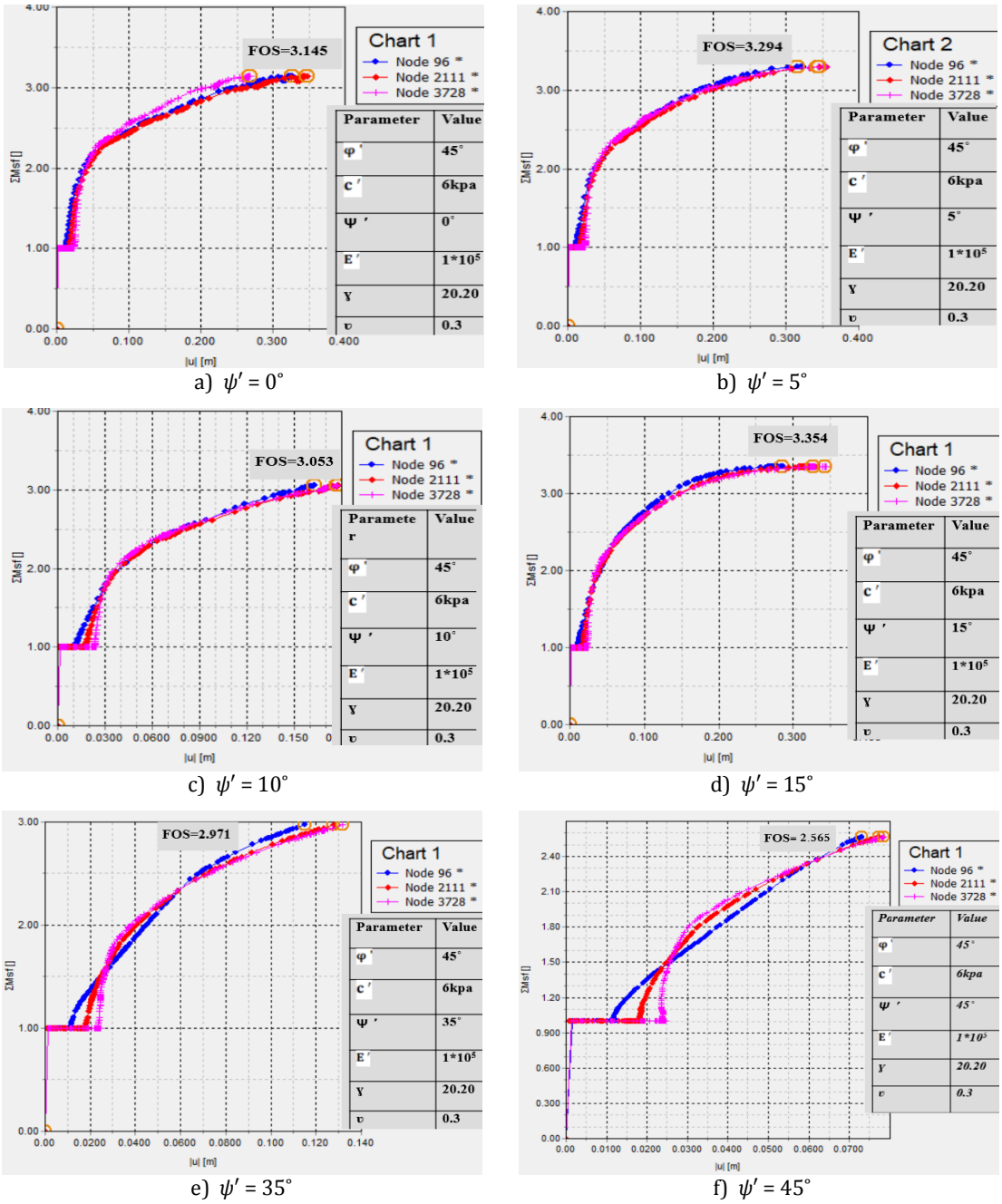

Fig. 6. Comparison of the *FoS* for framed prestressed anchor bar and sheet pile wall with different expansion angles.

Summarizing the above comparison from the two-dimensional model, Tschuchnigg and others believe that the model's trend is safe and stable. (Tschuchnig et al., 2015). When the expansion angle results, mesh roughness, and failure mechanism when compared, numerical values are different. Based on the two-dimensional model of (Tschuchnig et al., 2015) using PLAXIS 2D software, the slope model supported by frame prestressed anchor and sheet pile wall established, and the influence of expansion angle on slope stability is studied.

4.2. Deformation responses and effective stress

Deformation responses horizontal and vertical deformation responses were recorded at different locations of a framed prestressed anchor bar and sheet pile

wall. The values of horizontal distortion (0.08204) were found to be greater than the vertical distortion (0.03162) for all the cases considered. Hence, only vertical distortion differences are shown here. Fig. 7 displays the difference in vertical deformations of the framed prestressed anchor bar and sheet pile wall.

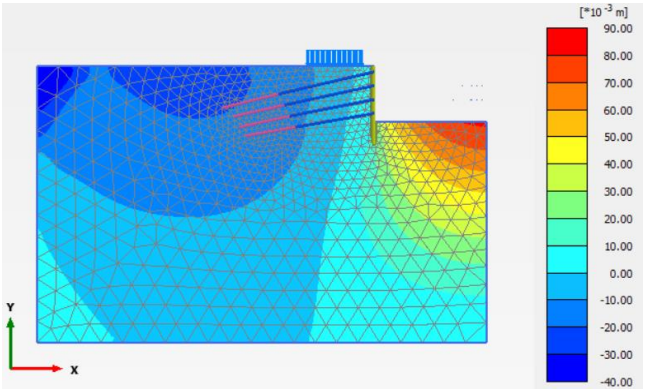

Fig. 7. Variation of vertical deformation of framed prestressed anchor bar and sheet pile wall.

Effective stress responses of effective stresses are recorded at a different location of framed prestressed anchor bar and sheet pile wall. The effective horizontal stress values are found to be more than that of effective vertical stress for all the considered cases. Typical variation of effective horizontal and vertical stresses of framed prestressed anchor bar and sheet pile wall presented in Figs. 8-10.

4.3. Discussion

4.3.1. Influence of expansion angle

The effects of expansion angles (ψ' = 0°, 5°, 10°, 15°, 35°, 45°) on the *FoS* affinity in the model were studied of a pre-framed anchor bar and two-dimensional laminate pile wall. The results showed that *FoS*=2.565 when ψ'=45° degrees, it shows higher instability than the two-dimensional model. The results show that *FoS* oscillations contract significantly (*FoS*=2.565) at 10°≤ ψ'≤ 35°, and the convergence is enhanced (almost no oscillation sign). For these cases, no significant difference in the destruction mechanism was more observed. When $\psi'=\varphi$, the *FoS* convergence and failure mechanism in the two-dimensional model are more evident than that in $\psi'\neq\varphi$ model. In the model, the results obtained in this study are different from those obtained by Tschuchnig et al. (2015). One they mean that the relevant flow-based (Davis, 1968) is not suitable for solving the slope stability problems in the pre-frame anchor bolt and two-dimensional laminate pile wall model. In the range of ψ'=35°-45°, the separation line events were observed in different affinity results of *FoS*. Therefore, the peak valley of ψ'=35° were analyzed to test the failure mechanism. When ψ'=35°, the failure surface is clear and developed; when ψ'= 45°, the failure surface is incomplete.

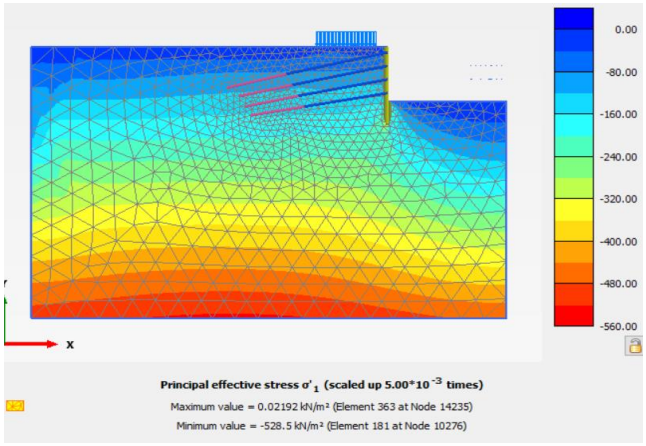

Fig. 8. Variation of effective stress of framed prestressed anchor bar and sheet pile wall (σ_1).

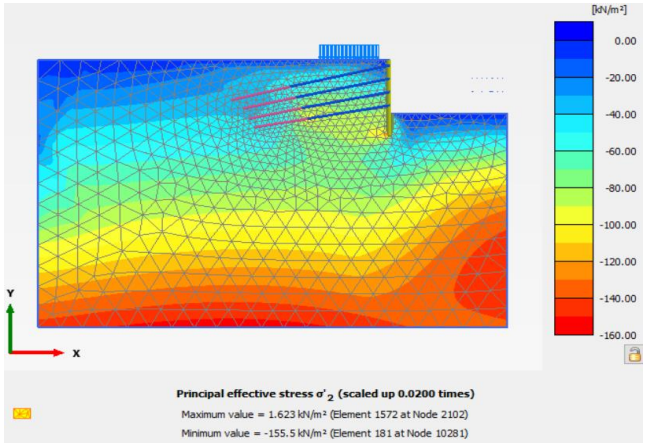

Fig. 9. Variation of effective stress of framed prestressed anchor bar and sheet pile wall (σ_2).

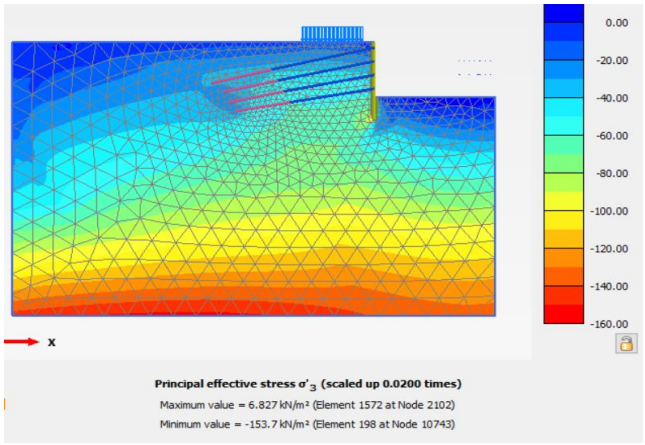

Fig. 10. Variation of effective stress of framed prestressed anchor bar and sheet pile wall (σ_3).

4.3.2. Effects of both pre-framed anchor tape and laminate pile wall and soil strength coefficients

The effect of the expansion angle on *FoS* affinity under different soil parameters was studied. For the friction

angle, since the numerical model must follow the balance rule (slope will not be a destroyed in its initial equilibrium state), a tilt angle (β=0°) is selected for inspection, and three different expansion angles (ψ'=0° and 15°) Degrees and ψ'=ψ. When the three-dimensional model was preparedness at β=0°, ψ'=0°, 15° and 45° are using to analyze various coherent quantities. When ψ'=0° or 15°, *FoS* affinity was relatively stable. According to the bound flow rule, the affinity at lower concentration is better than that at higher concentration-failure descent mechanism. Fig. 6 shows the effect of soil cohesion on *FoS* affinity; various c' convergence curves fluctuate slightly at low expansion angle (ψ'=0°). When ψ'=35°, most of the convergence curves are smooth except *c*'=20.02 kPa. For a high expansion angle (ψ'=45°), obvious oscillation with different *c* were observed. The trend observed in Fig. 6(d) and Fig. 6(e) is consistent, where converges smoothly when ψ'=15°-35°.

5. Conclusions

In this study, the influence of ψ' on *FoS* were analyzed by using frame prestressed anchor and sheet pile wall, and the PLAXIS 2D program was used to study the influence of ψ' on-grid roughness, inclination angle (β=0), and soil strength parameters (*c*' and ψ') through two-dimensional analysis of frame prestressed anchor and sheet pile wall. According to the results of this study, we can draw the following conclusions and suggestions.

- The results show that ψ' has a significant effect on *FoS* affinity, but this affinity may be unstable. However, the effects may vary depending on the inclination angle or soil strength parameters (*c*' and ψ').
- The expansion angle's influence on the slope model's convergence was supported by pre-frame anchor belts and laminated pile walls. On the other hand, various sliding surfaces. However, the two-dimensional model supported by pre-frame anchor tapes and laminated pile walls showed the opposite result-unstable at ϕ'=ψ'. Therefore, engineers must consider the influence of ψ' on *FoS* affinity.
- Declining soil strength parameters (*c*' and ϕ) compared with higher soil strength parameters, when ϕ'=ψ, the affinity of fiction *FoS* is relatively insensitive. Besides, when ψ'=ϕ'=45°, the tilt angle has little effect on the *FoS* affinity. However, when ψ'≠ϕ Depending on the value of ψ', the influence of the tilt angle ψ is different.

References

Baker R, Shukha R, Operstein V, Frydman S (2006). Stability charts for pseudo-static slope stability analysis. *Soil Dynamics and Earthquake Engineering*, 26(9), 813–823.

Bishop AW (1955). The use of slip circles in the stability analysis of earth slopes. *Geotechnique,* 5(1), 7–17.

Cai F, Ugai K, Hagiwara T (2002). Base stability of circular excavation in soft clay. *Journal of Geotechnical and Geoenvironmental Engineering,* 128(8), 702–706.

Cheng YM, Lansivaara T, Wei WB (2007). Two-dimensional slope stability analysis by limit equilibrium and strength reduction methods. Computers and Geotechnics, 34, 137–50.

Dafalias YF (1986). Bounding surface plasticity. I: Mathematical foundation and hypo- plasticity. *Journal of Engineering Mechanics*, 112 (9), 966–987.

Davis EH (1968). Theories of plasticity and failure of soil masses. In: *Lee IK, editor. Soil Mechanics: Selected Topics*. New York, NY, USA: Elsevier, 341–354.

Dawson EM, Roth WH, Drescher A (1999). Slope stability analysis by strength reduction. *Geotechnique*, 49(6), 835–840.

Griffiths DV (1999). Slope stability analysis by finite elements. *Geotechnique,* 49(3), 387-403.

Griffiths DV, Lane PA (2001). Slope stability analysis by finite elements. *Géotechnique,* 51(7), 653–654.

Griffiths DV, Marquez RM (2007). Three-dimensional slope stability analysis by elastic-plastic finite elements. *Geotechnique*, 57(6), 537–546.

Hang L, Ping C (2012). Influence of material dilation angle on stability of homogeneous with surcharge load. *International Journal of Geotechnical Engineering,* 17C, 329–340.

Ho IH (2014). Parametric studies of slope stability analyses using three-dimensional finite element technique: geometric effects. *Journal of GeoEngineering*, 9(1), 33–43.

Hwang J, Dewoolkar M, Ko HY (2002). Stability analysis of two-dimensional excavated slopes considering strength anisotropy. *Canadian Geotechnical Journal*, 39(5), 1026–1038.

Jerman J, Mašín D (2020). Hypoplastic and viscohypoplastic models for soft clays with strength anisotropy. *International Journal for Numerical and Analytical Methods in Geomechanics*, 44(10), 1396–1416.

Kolymbas D (2012). Barodesy: a new hypo plastic approach. *International Journal for Numerical and Analytical Methods in Geomechanics,* 36(9), 1220–1240.

Kumar J (2000). Slope stability calculations using limit analysis. In: *Proc. Slope Stability, ASCE Special Publication*, 101, 239–249.

Kumar J (2004). Stability factors for slopes with nonassociated flow rule using energy consideration. *International Journal of Geomechanics*, 264(4), 264–272.

Li AJ, Merifield RS, Lyamin AV (2010). Three-dimensional stability charts for slopes based on limit analysis methods. *Canadian Geotechnical Journal,* 47(12), 1316–1334.

Likitlersuang S, Pholkainuwatra P, Chompoorat T, Keawsawasvong S (2018). Numerical modelling of rail way embankment for high-speed train constructed on soft soil. *Journal of GeoEngineering*, 13(3), 149–159.

Lim K, Li AJ, Lyamin AV (2015). Three-dimensional slope stability assessment of two-layered untrained clay. *Computers and Geotechnics*, 70, 78–89.

Lim K, Lyamin AV, Cassidy MJ, Li AJ (2015). Three-dimensional slope stability charts for frictional fill materials placed on purely cohesive clay. *International Journal of Geomechanics*, 16(2), 04015042.

Lim K, Li AJ, Schmidt A, Lyamin AV (2017). Slope-stability assessments using finite-element limit-analysis methods. *International Journal of Geomechanics*, 17(2), 06016017.

Liu SY, Shao LT, Li HJ (2015). Slope stability analysis using the limit equilibrium method and two finite element methods. *Computers and Geotech*nics, 63, 291–298.

Lyamin A, Sloan S (2002b). Lower bound limit analysis using non-linear programming. *International Journal for Numerical Methods in Engineering*, 55(5), 573–611.

Lyamin AV, Sloan S (2002a). Upper bound limit analysis using linear finite elements and non-linear programming. *International Journal for Numerical and Analytical Methods in Geomechanics*, 26(2), 181–216.

Manzari MT, Nour MA (2000). Significance of soil dilatancy in slope stability analysis. *Journal of Geotechnical and Geoenvironmental Engineering*, 126(1), 75–80.

Matsui T, San KC (1992). Finite element slope stability analysis by shear strength reduction technique. *Soils Found*, 32(1), 59–70

Michalowski RL (2002). Stability charts for uniform slopes. *Journal of Geotechnical and Geoenvironmental Engineering*, 128(4), 351–355.

Morgenstern Nu, Price VE (1965). The analysis of the stability of general slip surfaces, *Geotechnique*, 15(1), 79–93.

Niemunis A, Herle I (1997). Hypoplastic model for cohesionless soils with elastic strain range. *Mechanics of Cohesive-frictional Materials: An International Journal on Experiments, Modelling and Computation of Materials and Structures*, 2(4), 279–299.

Roscoe KH (1970). The influence of strains in soil mechanics. *Geotechnique*, 20(2), 129–170.

Sulsky D, Zhou SJ, Schreyer HL (1995). Application of a particle-in-cell method to solid mechanics. *Computer Physics Communications*, 87(1–2), 236–252.

Tschuchnigg F, Schweiger HF, Sloan SW (2015). Slope stability analysis by means of finite element limit analysis and finite element strength reduction techniques. Part I: Numerical studies considering non-associated plasticity. *Computers and Geotechnics*, 70, 169–177.

Wu W, Kolymbas D (1990). Numerical testing of the stability criterion for hypo plastic constitutive equations. *Mechanics of Materials*, 9(3), 245–253.

Yu Y, Xie L, and Zhang B (2005). Stability of earth-rock fill dams: Influence of geometry on the three-dimensional effect. *Computers and Geotechnics*, 32(5), 326–339.

Zabala F, Alonso E (2011). Progressive failure of aznalcóllar dam using the material point method. *Géotechnique,* 61(9), 795–808.

Zienkiewicz OC, Humpheson C, Lewis RW (1975). Associated and non-associated visco-plasticity and plasticity in soil mechanics. *Geotechnique*, 25(4), 671–689.